Spin-flip Raman scattering, bound magnetic polaron, and fluctuations in (Cd,Mn)Se

D. Heiman

Francis Bitter National Magnet Laboratory, Massachusetts Institute of Technology,
Cambridge, Massachusetts 02139

P. A. Wolff and J. Warnock

Francis Bitter National Magnet Laboratory and Department of Physics,
Massachusetts Institute of Technology, Cambridge, Massachusetts 02139

(Received 26 October 1982)

The spin-flip energy of donor-bound electrons is investigated in the semimagnetic semiconductor $Cd_{1-x}Mn_xSe$. Temperature and magnetic field dependences are measured with the use of Raman scattering and calculated theoretically from a statistical-mechanical model. Results of spin-flip Raman scattering are obtained for $x = 0.01$ and 0.1 at temperatures from 1.5 to 30 K and fields to 10 T. For $x = 0.1$, the spin-flip energy is large (≤ 26 meV), giving g values approaching 200 at low temperatures. This enhancement is interpreted as an effective magnification of the field due to the exchange interaction between the carrier electron spin and the Mn^{2+} spins. The magnitude and temperature dependence of g are explained with the use of the mean-field approximation. At zero magnetic field the spin-flip energy is finite due to thermal fluctuations in the local magnetization and the bound magnetic polaron. These processes are incorporated in the theory which is used to derive simple formulas for the spin-flip energy and line shape. Good agreement is found between theory and experiment. The scattering strength and selection rules are also studied. The absolute cross section exceeds 10^{-20} cm^2/sr and is resonantly enhanced as the absorption edge is approached from lower energy.

I. INTRODUCTION

Recently, there have been a number of studies of the properties of semimagnetic semiconductors.[1] These materials—whose prototypes are $(Cd_{1-x}Mn_x)Te$ and $(Hg_{1-x}Mn_x)Te$—combine the features of conventional and magnetic semiconductors in novel and flexible ways. Their band structures are similar to those of the corresponding binary compounds (CdTe and HgTe). Transport properties are generally superior to those of magnetic semiconductors. Magnetically, semimagnetics exhibit a wide range of behavior[2] as a function of Mn concentration. Concentrated alloys ($x \gtrsim 0.2$) have spin-glass and antiferromagnetic phases. Dilute alloys are paramagnetic with modifications induced by the large exchange interactions of conduction- (or valence-) electron spins with those of the Mn^{2+} ions incorporated in the lattice. The exchange interaction gives rise to several novel effects, such as large spin splittings of the bands (giant g values). It also modifies localized states in these materials. An electron bound to a donor (or a hole to an acceptor) in a semimagnetic crystal polarizes the Mn^{2+} ions within its orbit, thus creating a ferromagnetic spin cloud around the impurity. Such complexes are termed bound magnetic polarons (BMP).

Spin-flip transitions of electrons in semimagnetic semiconductors were first observed by Raman scattering in (Hg,Mn)Te (Ref. 3) and (Cd,Mn)Se (Ref. 4). These transitions have also been seen in the far-infrared absorption spectra of (Cd,Mn)Se.[5] When it is detectable, spin-flip Raman scattering is a useful probe of the electronic structure of semimagnetic semiconductors. In particular, the observation[4] of a temperature-dependent zero-field spin splitting in (Cd,Mn)Se is a proof of the existence of BMP in that material. In this paper we describe the results of extensive spin-flip Raman scattering experiments in n-type (Cd,Mn)Se, and compare the data with a theory of BMP, which provides a complete description of the spin-flip line shape. Excellent agreement is found. This comparison substantiates the fluctuation-dominated picture of BMP developed by Dietl and Spałek.[6] Thermal fluctuations will be included whenever reference is made to BMP, even when the polaron contribution is small.

The measurements also provide an accurate value for the exchange interaction, and determine other parameters of the (Cd,Mn)Se system. A large

enhancement of the spin-flip cross section is observed as the laser energy approaches the absorption edge. Cross sections exceeding 10^{-20} cm^2/sr are measured at resonance.

II. EXPERIMENT

A. Samples and equipment

Samples of Cd$_{1-x}$Mn$_x$Se were grown by the Bridgman method with nominal x values of 1% and 10%. Actual values of the concentrations are only slightly different, as determined by atomic absorption measurements. At low Mn concentrations the crystals have the hexagonal wurtzite structure of pure CdSe. The energy gap for the A valence band at $x = 0$ is $E_g^A = 1841$ meV at $T = 4$ K, and varies with x. The variation is linear at least up to $x = 0.45$, with $dE_g/dx = 1.50$ eV at liquid-helium temperature.[7] Although the samples were not intentionally doped, they exhibited n-type conductivity with $n \simeq 10^{16}$–10^{18} cm^{-3} at room temperature. See Table I for material parameters.

Transport properties at room temperature were determined from the Hall effect using the four-point van der Pauw method. The low manganese concentration sample, $x = 0.012$, has a conductivity of $\sigma = 16$ (Ω cm)$^{-1}$ and $n = 2 \times 10^{17}$ cm^{-3}. The high-concentration sample, $x = 0.105$, has $\sigma = 2.2$ (Ω cm)$^{-1}$ and $n = 3 \times 10^{16}$ cm^{-3}. Both samples were polished to a thickness of 1.5 mm. All samples tested have wavelength-independent background absorption below the band gap. A sizable absorption was found in the $x = 0.1$ sample, for which $\alpha_0 = 16$

cm^{-1}. In the $x = 0.01$ sample $\alpha_0 = 2$ cm^{-1}. This absorption is attributed to impurities other than manganese. A third sample, grown by iodine transport, has $\alpha_0 \simeq 10^2$ cm^{-1}, presumably due to residual iodine impurities. No spin-flip scattering was found in this crystal.

Spin-flip energies were determined from spontaneous Raman scattering using a backscattering configuration. The incident light was produced by a tunable dye laser pumped by a Q-switched Nd:yttrium aluminum garnet laser having a 10-nsec pulse length at 10 pps repetition rate. The dye laser was tunable over the range $\hbar\omega_L = 1720$–1850 meV using LD688 dye, and from 1850 to 2000 meV with DCM dye from the Exciton Chemical Co. The dye-laser output was linearly polarized and focused to a slit image on the sample by a 25-cm—focal-length cylindrical lens. The intensity in the sample was between 10^5 and 10^7 W/cm^2. Data were only taken with intensities that did not produce sample heating. Samples were mounted in a variable-temperature, exchange-gas Dewar. The optical Dewar tail was mounted in a 100-kG Bitter-solenoid magnet permitting radial access to the field. Raman scattered light was collected in 10^{-2}-sr solid angle and focused onto the slit of a $\frac{3}{4}$-m double monochromator. Slit widths of 100 and 200 μm gave spectral resolutions of $R = 0.1$ and 0.2 meV, respectively. The scattered light was detected by a photomultiplier with GaAs photocathode and gated integrator. The laser photon energy $\hbar\omega_L$ was set 40–70 meV below the band gap in each sample to take advantage of resonance enhancement of the scattering cross section.

TABLE I. Parameters for Cd$_{1-x}$Mn$_x$Se.

Quantity	Symbol	Sample	Sample[a]	Sample	Units
Mn concentration	x	0.0122 ± 0.0014	0.05	0.105 ± 0.005	
Conductivity[b]	σ	16	2.78	2.2	(Ω cm)$^{-1}$
Hall mobility[b]	μ_H	490		470	$\dfrac{\text{cm}^2}{\text{V sec}}$
Carrier concentration[b]	n	2×10^{17}	4×10^{16c}	3×10^{16}	cm^{-3}
Slope $\partial \Delta E/\partial B$	m	1.01 ± 0.10		4.4 ± 0.4	$\dfrac{\text{meV K}}{\text{kG}}$
Antiferromagnetic temperature from $\tilde{g}$ from BMP	T_{AF}	0.9 ± 0.3	1.2^d	3.0 ± 0.6 2.2 ± 0.2	K K
Effective exchange energy	$(\alpha N_0)\tilde{x}$	2.6 ± 0.3	7.6^d	11.1 ± 0.6	meV

[a]From Nawrocki et al., Ref. 4.
[b]Room-temperature results.
[c]Calculated by assuming $\mu_H = 500$ cm^2/V sec.
[d]From Dietl and Spałek, Ref. 6.

B. Results of spin-flip energies in the mean-field range

The Stokes shift of the spin-flip Raman scattering peak, ΔE, is plotted as a function of applied magnetic field in Figs. 1 and 2, for $x = 0.01$ and 0.1, respectively. Results are shown for lattice temperatures between $T = 2$ and 30 K. These graphs omit the lowest-field region $(B \lesssim 2$ kG) where the electron's spin-flip energy is determined by BMP interactions. The BMP data will be discussed in Sec. VI. For fields beyond the BMP range, ΔE varies linearly with field, and ultimately saturates at high fields. The saturation is most evident in the $x = 0.01$ sample, as shown in Fig. 1. Here, ΔE clearly reaches a limit of 7 meV. As required by mean-field theory, at high temperatures larger fields are required to reach this limit. This limiting behavior is due to saturation of the manganese magnetization, described by the usual Brillouin function for paramagnetic ions with $S = \frac{5}{2}$. The same behavior is evident, though less clearly, in the $x = 0.1$ sample as shown in Fig. 2. Here, the limiting energy is much larger, nearly 26 meV.

The effective g values $(\Delta E = \tilde{g}\mu_B B)$ are quite large in both samples. At the lowest temperature, $T = 1.9$ K, $\tilde{g} = 70$ for the low-concentration, $x = 0.01$ sample, and $\tilde{g} = 170$ for the $x = 0.1$ sample. These values can be compared to that found in n-type CdSe where $g^* = 0.5$. The effective g value de-
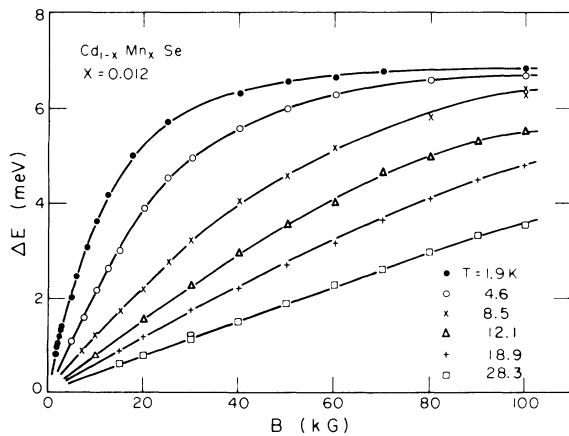

FIG. 2. Spin-flip Stokes energy ΔE vs applied magnetic field B from Raman scattering in $Cd_{1-x}Mn_xSe$, $x = 0.10$, for different lattice temperatures. Backscattering was used with polarization (xy), $\vec{B}||\hat{x}$, and $\hat{c}||\hat{z}$. The solid curves are drawn through the points for clarity.

FIG. 1. Spin-flip Stokes energy ΔE vs applied magnetic field B from spontaneous Raman scattering in $Cd_{1-x}Mn_xSe$, $x = 0.012$, for various lattice temperatures. A backscattering geometry was used with incident and scattered polarization (xz), $\vec{B}||\hat{x}$, and $\hat{c}||\hat{z}$. The solid lines are drawn to aid the eye.

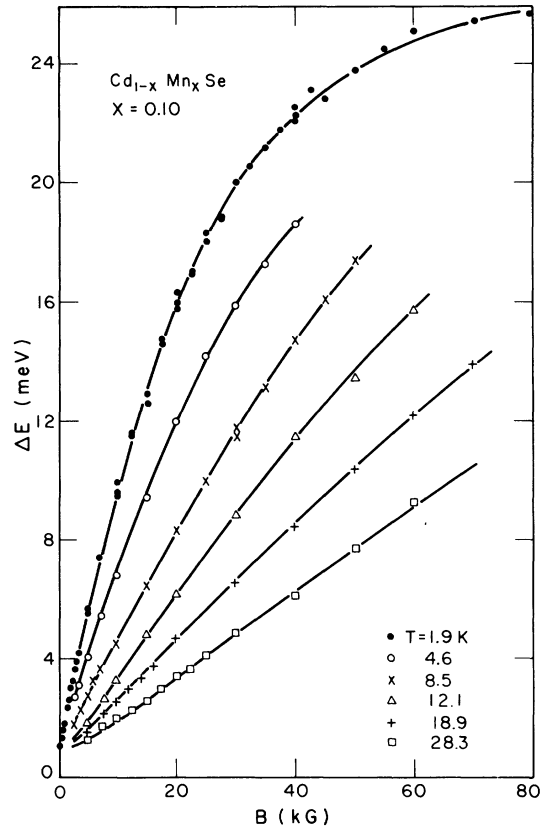rived from mean-field theory is given by[8]

$$\tilde{g} = g^* + \frac{35\bar{x}(\alpha N_0)}{12k(T + T_{AF})}g_{Mn} , \tag{1}$$

where $\bar{x}$ is the effective x value, (αN_0) the exchange energy, N_0 the density of cation sites, k the Boltzmann's constant, T the temperature, and $g_{Mn} = 2.0$. Both $\bar{x}$ and T_{AF} are due to antiferromagnetic (AF) interaction between Mn ions. The second term in Eq. (1) results from the electron-Mn^{2+} exchange interaction and dominates except at very low concentrations and very high temperatures. This term remains finite as $T \to 0$ because the Mn^{2+} susceptibility is limited by antiferromagnetic Mn^{2+}-Mn^{2+} coupling. Near $T = 0$, $\tilde{g}$ increases with increasing x for small x, but may eventually decrease at larger x. This effect occurs because both T_{AF} and $\bar{x}$ depend on x. For example, in $(Cd,Mn)Te$, T_{AF} increases in a roughly linear fashion with x, and $\bar{x}/x$
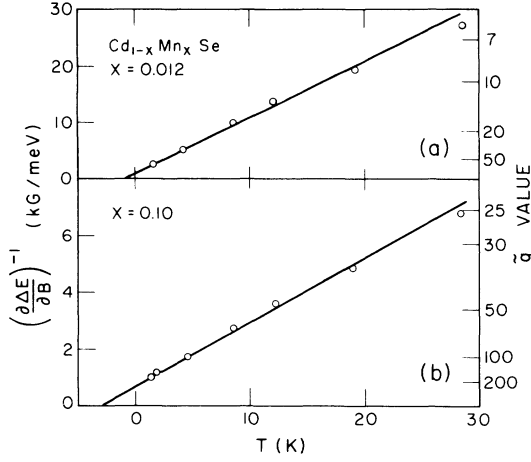
FIG. 3. $(\partial\Delta E/\partial B)^{-1}$ vs lattice temperature in $Cd_{1-x}Mn_xSe$ for $x=0.012$ and $x=0.10$. $\partial\Delta E/\partial B$ is the slope of the linear part of the ΔE-vs-B curves of Figs. 1 and 2. See Table I for parameters. The straight lines are fits to the experimental data.

decreases with x.[9]

In order to determine T_{AF} and $(\alpha N_0)\bar{x}$ in each sample, the inverse slope of the ΔE-vs-B curves are plotted in Fig. 3 as a function of temperature. Both samples show linear dependence of the form $\partial\Delta E/\partial B = m/(T+T_{AF})$. Fitting this function to the experimental points yields $m=1.01$ meV K/kG and $T_{AF}=0.9$ K for $x=0.01$, and $m=4.4$ meV K/kG and $T_{AF}=3.0$ K for $x=0.1$. The exchange constants determined from these are $(\alpha N_0)\bar{x}=2.6$ meV for $x=0.01$ and 11.2 meV for $x=0.1$. With the use of the value $\alpha N_0=260$ meV from magnetization measurements,[10] $\bar{x}/x=0.82$ for $x=0.01$ and $\bar{x}/x=0.41$ for $x=0.1$. The increase in T_{AF} and decrease in $\bar{x}/x$ for increasing x is due to an increased number of antiferromagnetic cancellations of near-neighbor Mn^{2+} ions.

III. THEORY

A. The BMP model

The Hamiltonian we will use to describe the BMP is a generalization of the Hamiltonian discussed by Golnik, Gaj, Nawrocki, Planel, and Benoît à la Guillaume[11] (GGNPB). The GGNPB model was developed to explain experiments in (Cd,Mn)Te, but should be equally applicable to other wide-gap semimagnetic semiconductors, such as (Cd,Mn)Se. The assumptions made in the GGNPB paper are the following:

(1) The localized electron (or hole) wave function has the form

$$\Psi(\vec{r})=F(\vec{r})u_0(\vec{r})$$

$$=\left[\frac{1}{\pi(a_0^*)^3}\right]^{1/2}e^{-r/a_0^*}u_0(\vec{r}),\qquad(2)$$

where $u_0(\vec{r})$ is the periodic, band-edge Bloch function.

(2) Modifications of this wave function due to interactions with Mn^{2+} ions are neglected.

(3) The exchange Hamiltonian of the system has a Heisenberg form. For electrons, the interaction is

$$\mathscr{H}_{exch}=-\alpha\sum_j[(\vec{s}\cdot\vec{S}_j)|F(\vec{R}_j)|^2].\qquad(3)$$

Here $\vec{s}$ is the electron spin, α the exchange integral, and $\vec{R}_j$ and $\vec{S}_j$ are the positions and spins of the Mn^{2+} ions.

(4) The Mn^{2+}-ion system, considered separately, is perfectly paramagnetic. Magnetic susceptibility data suggest that this approximation is valid for temperatures exceeding 1–2 K.

(5) The electron is assumed to be totally spin polarized $(s_z=\frac{1}{2})$.

The assumptions of GGNPB are valid in some of the experiments referenced above, but quite questionable in others. For example, in the more concentrated $(Cd_{1-x}Mn_x)Te$ samples studied by GGNPB, the exchange-induced portion of the exciton binding energy exceeds the Coulombic part. This result suggests considerable modification of the acceptor wave function. Similarly, in the $(Cd_{1-x}Mn_x)Se$ spin-flip experiments, the approximation of complete spin polarization $(s_z=\frac{1}{2})$ breaks down in the high-temperature, low-field range. These difficulties can be circumvented with an extension of the GGNPB model, and a more accurate evaluation of the partition function or correlation function. In particular, we will demonstrate below that the exchange Hamiltonian remains valid, even with considerable distortion of the BMP wave function, provided that $F(\vec{r})$ is determined in a self-consistent way from a suitably spin-averaged exchange interaction.

Consider the case of donor BMP such as those observed[4] in (Cd,Mn)Se. These complexes are simpler than the acceptor polarons studied by GGNPB because the conduction-band edge of II-VI compounds is nondegenerate, whereas in cubic II-VI crystals the valence-band edge has the degeneracy implied by Γ_8 symmetry. Nevertheless, many of the ideas developed below should also apply to the degenerate-band situation. The effective-mass Hamiltonian for a donor BMP is

$$\mathscr{H}=\left[\frac{p^2}{2m^*}\right]-\left[\frac{e^2}{\epsilon_0 r}\right]-\alpha\sum_j[(\vec{s}\cdot\vec{S}_j)\delta(\vec{r}-\vec{R}_j)].$$
$$(4)$$

Here, the small ($\simeq 5\%$) mass and dielectric constant anisotropies of n-type, hexagonal II-VI crystals are neglected. Equation (4) describes the motion of an electron in a Coulomb potential plus random exchange potential due to the Mn^{2+} ions. The latter can scatter the electron from one orbital state to another. In practice, however, scattering occurs infrequently. A Born-approximation calculation yields a mean free path for (Cd,Mn)Se:

$$\lambda \simeq \left[\frac{1}{x}\right]\left[\frac{m_0}{m*}\right]^2 10^{-6} , \tag{5}$$

in units of cm. This estimate assumes $(\alpha N_0)\simeq 0.2$ eV. In a (Cd,Mn)Se sample containing 10% Mn, the mean free path is about 10^3 times the Bohr radius. The electron circles the charged impurity many times before scattering. This result implies that donors in semimagnetics have reasonably well-defined orbital levels, despite the presence of scatterers.

The relative weakness of the Mn^{2+} scattering suggests a Hartree-type approximation for the BMP wave function:

$$\Psi(\vec{r},\vec{s};\vec{S}_j) \simeq F(\vec{r})\chi(\vec{s};\vec{S}_j) . \tag{6}$$

Here $F(\vec{r})$ is the orbital donor state and $\chi(\vec{s};\vec{S}_j)$ is a spinor describing the interaction of the electron spin with those of Mn^{2+} ions within its orbit. The spin

Hamiltonian that determines χ is obtained by multiplying the Schrödinger equation by $F^*(\vec{r})$ and integrating over coordinates. The result is

$$\mathcal{H}_{spin}\chi \equiv \left[E_x - \alpha\sum_j [(\vec{s}\cdot\vec{S}_j)|F(\vec{R}_j)|^2]\right]\chi = E\chi , \tag{7}$$

where

$$E_x = \int F^*(\vec{r})\left[\frac{p^2}{2m*} - \frac{e^2}{\epsilon_0 r}\right]F(\vec{r})d^3r \tag{8}$$

is the usual donor energy.

In the standard Hartree theory the wave function is determined by minimizing the energy with respect to wave functions of a certain form. The BMP has an enormous number of accessible spin states, even at temperatures well below 1 K. Thus it is more appropriate to minimize the free energy

$$G = -kT\ln(Z) , \tag{9}$$

$$Z = \text{Tr}(e^{-\beta\mathcal{H}_{spin}}) , \tag{10}$$

[where $\beta \equiv (kT)^{-1}$] with respect to $F^*(\vec{r})$, subject to the normalization condition

$$N \equiv \int |F(\vec{r})|^2 d^3r = 1 . \tag{11}$$

The result is

$$\left[\frac{\delta G}{\delta F^*(\vec{r})} - \epsilon\frac{\delta N}{\delta F^*(\vec{r})}\right] = Z^{-1}\underset{(spins)}{\text{Tr}}\left[\frac{\delta\mathcal{H}_{spin}}{\delta F^*(\vec{r})}e^{-\beta\mathcal{H}_{spin}}\right] - \epsilon F(\vec{r})$$

$$= \left[\frac{p^2}{2m*}\frac{e^2}{\epsilon_0 r} - \alpha\sum_j [\langle\vec{s}\cdot\vec{S}_j\rangle\delta(\vec{r}-\vec{R}_j)] - \epsilon\right]F(\vec{r}) = 0 , \tag{12}$$

where

$$\langle\vec{s}\cdot\vec{S}_j\rangle = Z^{-1}\underset{(spins)}{\text{Tr}}[(\vec{s}\cdot\vec{S}_j)e^{-\beta\mathcal{H}_{spin}}] . \tag{13}$$

Equation (12) is a Schrödinger equation, in coordinate space, that determines $F(\vec{r})$. To solve it one must evaluate the spin average $\langle\vec{s}\cdot\vec{S}_j\rangle$ which, in turn, involves $F(\vec{r})$ through the spin Hamiltonian. Thus Eqs. (7), (12), and (13) are a coupled set that must be solved self-consistently to determine $F(\vec{r})$ and $\langle\vec{s}\cdot\vec{S}_j\rangle$. In practice, this calculation may be done variationally.

B. The spin-spin correlation function

The spin-flip spectrum $S(\omega)$ is the Fourier transform of the time-dependent, spin-spin correlation function[12]:

$$S(\omega) = \int_{-\infty}^{\infty} S(t)e^{i\omega t}\frac{dt}{2\pi} , \tag{14}$$

with

$$S(t) = \langle[\vec{s}(t)\cdot\vec{\alpha}][\vec{s}(0)\cdot\vec{\alpha}^*]\rangle$$
$$= Z^{-1}\text{Tr}\{[\vec{s}(t)\cdot\vec{\alpha}][\vec{s}(0)\cdot\vec{\alpha}^*]e^{-\beta\mathcal{H}}\} . \tag{15}$$

Here,

$$\vec{s}(t) \equiv e^{i\mathcal{H}t}\vec{s}(0)e^{-i\mathcal{H}t} , \tag{16}$$

and

$$Z = \text{Tr}(e^{-\beta\mathcal{H}}) . \tag{17}$$

As discussed in Ref. 11, the unit vector $\vec{\alpha}$ is deter-

mined by the geometry of the scattering experiment and the laser frequency. For our purposes, $\vec{a}$ can be viewed as a constant—involving neither the electron nor Mn^{2+} spin variables.

To calculate $S(\omega)$ for the BMP we generalize the GGNPB spin Hamiltonian [Eq. (3)] to include the effects of a dc magnetic field. In this approximation

$$\mathcal{H} = - \sum_j [K_j(\vec{s}\cdot\vec{S}_j)] - \mu g^*(\vec{s}\cdot\vec{B}_0)$$

$$- \mu g_{Mn} \sum_j [(\vec{S}_j\cdot\vec{B}_0)] \; , \tag{18}$$

where

$$K_j \equiv \alpha \, | F_0(\vec{R}_j) |^2 \; . \tag{19}$$

This expression for $\mathcal{H}$ can be abbreviated via the definition

$$\vec{\Gamma} \equiv \sum_j (K_j\vec{S}_j) + \mu g^*\vec{B}_0 \; . \tag{20}$$

Physically, $\vec{\Gamma}/\mu g^*$ is the "effective field" experi-

enced by the electron. $\vec{\Gamma}$ is a vector operator whose components do not commute with one another. This fact precludes an exact evaluation of the traces in Eqs. (15) and (17). However, the individual Mn^{2+} spins are fairly large $(S = \frac{5}{2})$, and in the BMP they are combined to give a net moment of many Bohr magnetons. Thus $\vec{\Gamma}$ is nearly a classical variable. The accuracy of the classical approximation is discussed in the Appendix for a simplified model of the BMP. It is there shown that the error is of order $N^{-1/2}$, where N is the number of Mn^{2+} ions within the BMP orbit.

In the classical approximation

$$e^{-\beta\mathcal{H}} \simeq \exp\left[\beta\mu g_{Mn} \sum_j (\vec{S}_j\cdot\vec{B}_0)\right] e^{\beta(\vec{s}\cdot\vec{\Gamma})} \tag{21}$$

and

$$e^{i\mathcal{H}t} \simeq e^{-i(\vec{s}\cdot\vec{\Gamma})t} \exp\left[-i\mu g_{Mn} \sum_j (\vec{S}_j\cdot\vec{B}_0)t\right] \; . \tag{22}$$

The expression for $S(t)$ simplifies to the form

$$S(t) \simeq Z^{-1} \text{Tr} \int \delta(\vec{\gamma}-\vec{\Gamma})d^3\gamma \left[\exp\left[\beta\mu g_{Mn} \sum_j (\vec{S}_j\cdot\vec{B}_0)\right] e^{\beta(\vec{s}\cdot\vec{\gamma})}[\vec{s}(t)\cdot\vec{a}][\vec{s}(0)\cdot\vec{a}^*]\right] \; . \tag{23}$$

The time-dependent spin operator in Eq. (23) can be evaluated by rewriting $(\vec{s}\cdot\vec{a})$ in terms of stepping-up and stepping-down operators with respect to the direction $\vec{\gamma}$. The calculation is outlined in the Appendix. With that result, the trace over spin variables in Eq. (23) is performed with the aid of the identity

$$e^{\beta(\vec{s}\cdot\vec{\gamma})} \equiv \left[\cosh\left[\frac{\beta\gamma}{2}\right] + \frac{2(\vec{s}\cdot\vec{\gamma})}{\gamma}\sinh\left[\frac{\beta\gamma}{2}\right]\right] \; . \tag{24}$$

Straightforward algebra yields the relation

$$\text{Tr}_{\{\vec{s}\}} \{e^{\beta(\vec{s}\cdot\vec{\gamma})}[\vec{s}(t)\cdot\vec{a}][\vec{s}(0)\cdot\vec{a}^*]\}$$

$$= \left[\left[\frac{(\vec{\gamma}\cdot\vec{a})(\vec{\gamma}\cdot\vec{a}^*)}{\gamma^2}\cosh\left[\frac{\beta\gamma}{2}\right] + \frac{1}{4}\left[(\vec{a}\cdot\vec{a}^*) - \frac{(\vec{\gamma}\cdot\vec{a})(\vec{\gamma}\cdot\vec{a}^*)}{\gamma^2} - \frac{i\vec{\gamma}\cdot(\vec{a}\times\vec{a}^*)}{\gamma}\right]e^{i\gamma t}e^{-\beta\gamma/2}\right.$$

$$\left. + \frac{1}{4}\left[(\vec{a}\cdot\vec{a}^*) - \frac{(\vec{\gamma}\cdot\vec{a})(\vec{\gamma}\cdot\vec{a}^*)}{\gamma^2} + \frac{i\vec{\gamma}\cdot(\vec{a}\times\vec{a}^*)}{\gamma}\right]e^{-i\gamma t}e^{\beta\gamma/2}\right] \equiv T(t;\vec{\gamma};\beta) \; . \tag{25}$$

The trace over electron spin variables has here been separated (via the classical approximation) from that over Mn^{2+} spins.

Finally, the trace over $\{\vec{S}_j\}$ is evaluated after substituting Eq. (25) into Eq. (23). The expression for $S(t)$ then takes the form

$$S(t) = Z^{-1} \text{Tr}_{\{\vec{S}_j\}} \int \int \frac{d^3\gamma d^3\lambda}{(2\pi)^3} \left[\exp[i\vec{\lambda}\cdot(\vec{\gamma}-\vec{\Gamma})] \exp\left[\beta\mu g_{Mn} \sum_j (\vec{S}_j\cdot\vec{B}_0)\right] T(t;\vec{\lambda};\beta)\right]$$

$$= Z^{-1}(6)^{N_1} \int \int \frac{d^3\gamma d^3\lambda}{(2\pi)^3} \left[\exp[i\vec{\lambda}\cdot(\vec{\gamma}-\mu g^*\vec{B}_0)] \prod_j [\mathscr{F}_{5/2}(\, |\beta\mu g_{Mn}\vec{B}_0 - i\vec{\lambda}K_j| \,)] T(t;\vec{\lambda};\beta)\right] \; . \tag{26}$$

N_1 is the number of Mn^{2+} spins in the sample, and

$$\mathcal{F}_{5/2}(x) \equiv \tfrac{1}{6}(e^{5x/2} + e^{3x/2} + e^{x/2} + e^{-x/2} + e^{-3x/2} + e^{-5x/2}) .$$ (27)

For small x

$$\mathcal{F}_{5/2}(x) \simeq (1 + \tfrac{35}{24}x^2) .$$ (28)

Equation (26) is a complicated result, but simplifies when $\mathcal{F}_{5/2}(x)$ is replaced by Eq. (28). This approximation is valid [in the (Cd,Mn)Se case] for temperatures above 1 K and fields below saturation values. We find

$$S(t) \simeq C \int \int \frac{d^3\gamma \, d^3\lambda}{(2\pi)^3} \{\exp[i\vec{\lambda}\cdot(\vec{\gamma}-\mu\tilde{g}\vec{B}_0)]e^{\lambda^2/2W_0^2}T(t;\vec{\gamma};\beta)\}$$

$$= C \int d^3\gamma \left[\frac{\exp[-(\vec{\gamma}-\mu\tilde{g}\vec{B}_0)^2/2W_0^2]}{(2\pi W_0^2)^{3/2}} T(t;\vec{\gamma};\beta) \right] ,$$ (29)

where

$$\tilde{g} = g^* + \tfrac{35}{12}g_{Mn}\beta \sum_j K_j = g^* + \tfrac{35}{12}g_{Mn}\frac{\bar{x}(\alpha N_0)}{k(T+T_{AF})} ,$$ (30)

$$W_0^2 = \tfrac{35}{12}\sum_j K_j^2 = \frac{35}{96}\frac{\bar{x}(\alpha N_0)^2}{\pi(a_0^*)^3 N_0} .$$ (31)

The weak antiferromagnetic Mn-Mn interactions have been incorporated phenomenologically by introducing $\bar{x}$ and T_{AF}. The constant C is given by the equation

$$C = Z_1^{-1}(6)^{N_1}\exp[\tfrac{35}{24}N_1\beta^2(\mu g_{Mn}B_0)^2] .$$ (32)

The second factor in Eq. (30) describes the internal field exerted by the Mn^{2+} spins (via the exchange interaction) on the electron spin. The temperature dependence of $\tilde{g}$ reflects the degree of Mn^{2+} spin alignment. Equation (30) implies that electrons in semimagnetics have enhanced g values—this is the conventional way of describing the electron-Mn^{2+} interaction. Physically, however, the effect is better viewed as a *magnetic field amplification*. Amplification factors exceed 300 at low temperatures. Thus a 10-kG field applied to (Cd,Mn)Se can give rise to effects that would require a 10^3-kG field in pure CdSe.

In the following, the replacement $W_0 \rightarrow W$ is made, where W is the characteristic energy of the BMP and is later related to W_0. $W/\mu g_{Mn}$ is the root-mean-square fluctuation of the internal field about its equilibrium value. For $(Cd_{1-x}Mn_x)Se$ with $x = 0.1$, W_0 is 0.66 meV, corresponding to a rms internal field fluctuation of 200 kG. These fluctuations are responsible for the observed BMP spin-flip linewidths.

The Fourier transform of Eq. (29) determines the spin-flip spectrum

$$S(\omega) = C \int d^3\gamma \frac{\exp[-(\gamma-\mu\tilde{g}B_0)^2/2W^2]}{(2W^2)^{3/2}}$$

$$\times \left[\frac{(\vec{\gamma}\cdot\vec{a})^2}{\gamma^2}\cosh\left[\frac{\beta\gamma}{2}\right]\delta(\omega) + \frac{1}{4}\left[(\vec{a}\cdot\vec{a}^*) - \frac{|(\vec{\gamma}\cdot\vec{a})|^2}{\gamma^2} + \frac{i\vec{\gamma}\cdot(\vec{a}\times\vec{a}^*)}{\gamma}\right]e^{\beta\omega/2}\delta(\gamma-\omega) \right.$$

$$\left. + \frac{1}{4}\left[(\vec{a}\cdot\vec{a}^*) - \frac{|(\vec{\gamma}\cdot\vec{a})|^2}{\gamma^2} - \frac{i\vec{\gamma}\cdot(\vec{a}\times\vec{a}^*)}{\gamma}\right]e^{\beta\omega/2}\delta(\gamma+\omega) \right] .$$ (33)

We are primarily interested in the second and third terms of Eq. (24), which describe Stokes and anti-Stokes spin-flip scattering. The first zero-frequency term causes Faraday rotation.[13] We will not discuss it here.

The integrals appearing in Eq. (33) are generally tedious to evaluate. They simplify, however, in the limiting cases $B_0 = 0$ and $\mu\tilde{g}B_0 \gg W$. For the zero-field case, the spectrum has the form

$$S_0(\omega) \sim \omega^2 e^{-\omega^2/2W^2}e^{\beta\omega/2} .$$ (34)

Here, ω ranges from $-\infty$ to ∞: Positive frequen-

cies correspond to Stokes scattering, negative ones to anti-Stokes scattering. As discussed in Sec. VI, Eq. (34) gives an excellent fit to the measured, zero-field spin-flip line shape.

It is interesting to compare this spectrum with that proposed[6] by Dietl and Spałek (DS). The key suggestion of their paper is that the total probability—Stokes plus anti-Stokes—for observing a spin-flip transition whose frequency shift has magnitude ω is determined by a Ginzburg-Landau free-energy functional (F) via the relation

$$[S_0(\omega)+S_0(-\omega)]$$

$$\simeq \int e^{-\beta F(\Delta)}\delta(\omega-\Delta)d^3\Delta \sim \omega^2 e^{-\beta F(\omega)} . \quad (35)$$

Equations (34) and (35) imply that

$$F(\omega)=\frac{kT\omega^2}{2W^2}-kT\ln\left[2\cosh\left[\frac{\omega}{2kT}\right]\right]$$

$$=\frac{4(\mu g_{Mn})^2(\pi a_0^{*3})\omega^2}{\alpha^2\chi}$$

$$-kT\ln\left[2\cosh\left[\frac{\omega}{2kT}\right]\right], \quad (36)$$

where χ is the susceptibility of the Mn^{2+} spin system. This function is precisely that used by DS [their Eqs. (2) and (3)] to describe the magnetic portion of the BMP free energy. Thus our theory is equivalent to theirs—though derived in a quite different way. In particular, $W^2=4kT\epsilon_p$, where ϵ_p is the characteristic energy of DS. The correspondence enabled us to correct Eq. (34) for the effects of direct Mn^{2+}-Mn^{2+} interactions. As DS emphasize, the first term in Eq. (36) describes the fluctuations of the Mn^{2+} magnetization about its equilibrium value. It is well known[14] that the magnitude of these fluctuations is determined by the susceptibility.

Equation (29) was derived on the assumption that the Mn^{2+} spins are noninteracting, i.e., that they have a Curie-type susceptibility. To correct for the observed weak antiferromagnetic interactions between them, one makes use of

$$W^2\equiv W_0^2\chi/\chi_{Curie}=W_0^2\left[\frac{T}{T+T_{AF}}\right] \quad (37)$$

in Eq. (34). This procedure was used in comparing the experimental data with theory (Sec. VI).

Finally, we consider the high-field spectrum ($\mu\tilde{g}B_0 \gg W$). In this limit, γ can be approximated by $\mu\tilde{g}B_0$ in the angular factors in Eq. (24). The remaining integral gives the spectrum

$$S_{high}(\omega)=\left[\left[\frac{W^2}{\mu\tilde{g}B_0\omega}\right]\sinh\left[\frac{\mu\tilde{g}B_0\omega}{W^2}\right]\right]S_0(\omega) .$$

$$(38)$$

This result smoothly extrapolates to $S_0(\omega)$ as $B_0\rightarrow 0$. In fact, Eq. (38) provides a good approximation to the spectrum over the whole field range below saturation, $0<\mu g_{Mn}B_0<kT$.

IV. RESULTS

A. Bound magnetic polaron and fluctuation regime

Effects due to the BMP are seen at low fields in the ΔE-vs-B data of Fig. 4 for $x=0.1$. As the field decreases, the linear behavior eventually gives way to a constant ΔE. This effect is more pronounced at higher temperatures; at $T=1.9$ K, ΔE is linear in B above 200 G, while at $T=18$ K linearity is not reached until $B=4$ kG. As B approaches zero, ΔE becomes constant at approximately 1 meV.

At $B=0$, the shift ΔE and linewidth (full width at half maximum) are plotted as a function of temperature in Fig. 5. Both ΔE and γ show little change from $T=5$ to 30 K. Below $T=5$ K, ΔE increases slightly while γ decreases. The shift and linewidth are described theoretically by Eq. (34). The theory is given by the solid curves using $W_0=0.66$ meV and $T_{AF}=2.3$ K. The experimental points are fit quite well considering the large
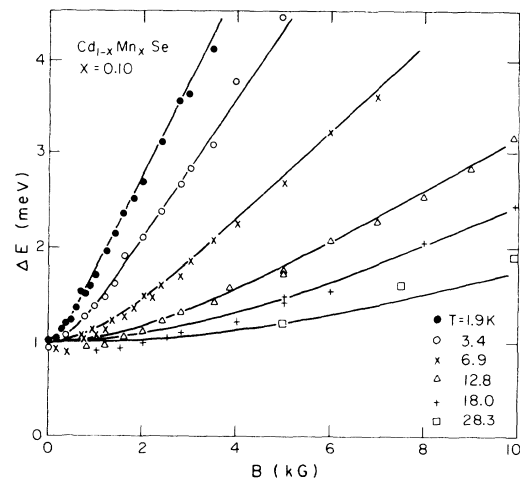

FIG. 4. Spin-flip Stokes energy ΔE-vs-B field from Raman scattering in $Cd_{1-x}Mn_xSe$, $x=0.10$, for different lattice temperatures. The solid curves were generated from the theory as described in the text with $W_0=0.66$ meV, $T_{AF}=2.3$ K, and $(\alpha N_0)\bar{x}=11.1$ meV.
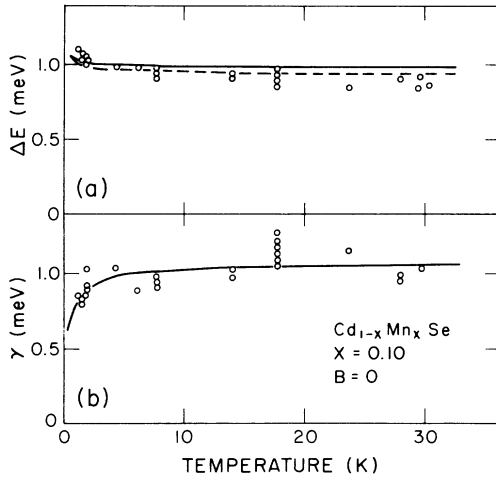
FIG. 5. Spin-flip energy ΔE and linewidth γ (full width at half maximum) at $B = 0$ from Raman scattering in $Cd_{1-x}Mn_xSe$, $x = 0.10$, vs lattice temperature. (Same geometry as in Fig. 2.) The curves were generated from the theory described in the text using $W_0 = 0.66$ meV and $T_{AF} = 2.3$ K. In the ΔE plot, the solid curve is the line center at half-maximum intensity and the dashed curve is the position of the peak of the line shape.

linewidth. It is difficult to determine ΔE accurately because of the large linewidth; ΔE can only be measured to within about one-tenth of the linewidth, or ± 0.1 meV. The linewidth is more uncertain. Although most of the experimental spectra show the peak to be clearly resolved, Fig. 6, the half-maximum position is usually obscured by the laser line at small frequency shifts. The linewidth is thus
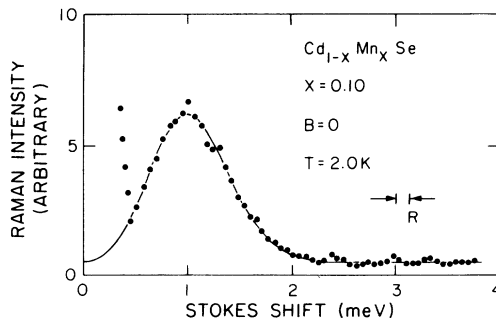

FIG. 6. Spectral line shape from spin-flip Raman scattering in $Cd_{1-x}Mn_xSe$, $x = 0.10$. The solid points are experimental determinations at $B = 0$ and lattice temperature $T = 2.0$ K. The instrumental resolution is $R = 0.1$ meV. The geometry used is the same as Fig. 2. The solid curve is from the theory discussed in the text with $W_0 = 0.66$ meV and $T_{AF} = 2.3$ K.

determined from only one-half the line shape. The uncertainty in γ is estimated at ± 0.2 meV.

The field dependence of ΔE, Fig. 4, is also fit quite well by the same W_0 and T_{AF} values determined from the $B = 0$ fit. The solid curves were derived using $W_0 = 0.66$ meV and $T_{AF} = 2.3$ K. The spectral line shape of Eq. (34) is shown in Fig. 6 along with the experimental points. The theoretical line shape fits the near-Gaussian experimental profile. The linewidth of the $x = 0.01$ sample is approximately 0.6 meV.

The value $W_0 = 0.66 \pm 0.07$ meV obtained by fitting ΔE at low fields can be compared to that calculated from Eq. (31). With the use of $\bar{x}(\alpha N_0) = 11.1$ meV, $(\alpha N_0) = 260$ meV, $a_0^* = 38$ Å, and $N_0 = 1.83 \times 10^{22}$ cm^{-3}, we find that $W_0 = 0.56 \pm 0.06$ meV, in reasonable agreement with the experimental value.

B. Scattering intensity

The Raman selection rules were determined in a backscattering geometry. Both samples showed identical selection rules appropriate to donor-bound electrons as determined by Thomas and Hopfield.[15] The observed nonzero tensor elements for $\hat{c}$ along $\hat{z}$ are the following: (xz) for $\vec{B}||\hat{c}$; (xx) and (xz) for $\vec{B}\perp\hat{c}$. The elements (xx) for $\vec{B}||\hat{c}$, and (zz) for both $\vec{B}||\hat{c}$ and $\vec{B}\perp\hat{c}$ were absent. These selection rules should be compared to those for free electrons given by[16] (ij), where $i \neq j$ and either i or j is parallel to $\vec{B}$.

The spin temperatures T_s were determined from the ratio of Stokes to anti-Stokes scattering. Spin temperatures were very different between the low- and high-n samples. The low carrier-concentration sample $n = 3 \times 10^{16}$ cm^{-3} ($x = 10\%$) showed good spin thermalization with the lattice temperature, even for incident light intensities as large as 10 MW/cm^2. The high carrier-concentration sample $n = 2 \times 10^{17}$ cm^{-3} ($x = 1\%$) showed spin temperatures much larger than the lattice temperature. The spin temperature varied from 20 to 120 K depending on the laser intensity. At large intensities the Stokes line becomes stimulated[17] and the spin temperature is not determined.

Resonance enhancement of the spin-flip Raman scattering from impurity-bound carriers has been described by Thomas and Hopfield.[15] The result for many intermediate states near resonance is

$$\frac{d\sigma}{d\Omega} = \left[\frac{e^2}{mc^2}\right]^2 \left[\sum_i f_i \frac{\hbar\omega_L/2}{E_i - \hbar\omega_L}\right]^2, \quad (39)$$

where the first factor is the Thomson cross section for free electrons, and f_i is the oscillator strength for an intermediate state at energy E_i. CdSe has

many intermediate states near the absorption edge. For an n-type sample, there are two free-exciton states, one each for the A and B valence bands, and two donor-bound exciton (I_2) states. The spin-orbit split valence band C is neglected since it lies 430 meV below the A band. The bound exciton contributes much more than the free excitons since the oscillator strength for bound excitons is much larger. (For example, in CdS, $f = 9$ for the I_2^A bound exciton, while $f = 2 \times 10^{-3}$ for free excitons.[15]) Thus only the two bound excitons I_2^A and I_2^B, which are separated by 25 meV, are important. The contribution from I_2^B is neglected for the energy range of the present experiment, since it amounts to, at most, one-third for small $\hbar\omega_L$. Finally, the one-level approximation near resonance gives

$$\frac{d\sigma}{d\Omega} = \left[\frac{e^2}{mc^2}\right]^2 f^2 \left[\frac{(E_I/2)^2}{(E_I - \hbar\omega_L)^2 + \Gamma^2}\right], \quad (40)$$

where Γ is a phenomenological broadening parameter. This result can be compared to that for scattering from free electrons, where f is replaced by $g^*/2$ and E_I by E_g.

The Raman scattering strength was found to vary dramatically near the absorption edge in both samples. The $x = 10\%$ sample at low temperature and at $B = 0$ showed a factor-of-220 increase in scattering cross section, going from $\hbar\omega_L = 1860$ to 1945 meV. The scattering was corrected for sample absorption in this region. Figure 7 shows the corrected scattering strength S as a function of laser photon energy. The quantity $S^{-1/2}$ is plotted to demonstrate the resonance denominator form
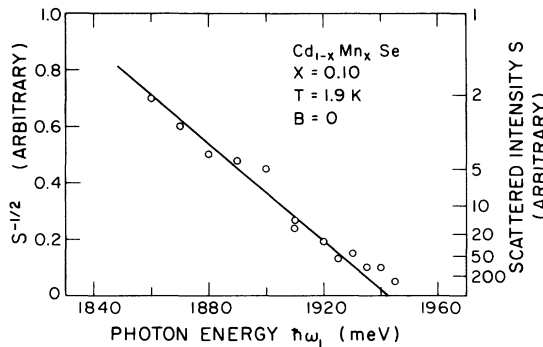

FIG. 7. Stokes-scattered intensity S vs laser photon energy $\hbar\omega_L$ in $Cd_{1-x}Mn_xSe$, $x = 0.10$, from spin-flip Raman scattering. A backscattering geometry was used with polarization (xy) and $\hat{c} \| \hat{z}$. The lattice temperature is $T = 1.9$ K and $B = 0$. S is corrected for sample absorption. The solid straight line is representative of $S \propto (E_I - \hbar\omega_L)^{-2}$, where $E_I = 1942$ meV.

$S \propto (E_I - \hbar\omega_L)^{-2}$. This dependence is shown by the straight line extrapolating to $E_I = 1942 \pm 5$ meV, which coincides with the absorption edge $(\alpha = 30$ cm$^{-1})$. The scattering strength is somewhat less very near E_I, where $S \propto [(E_I - \hbar\omega_L)^2 + \Gamma^2]^{-1}$. The experimental points can be fit by taking a Γ between 5 and 10 meV. The $n = 2 \times 10^{17}$ cm^{-3} sample also showed large resonance enhancement. The quantitative enhancement was less clear because of intensity-dependent effects, due to stimulated scattering. However, the shift of the stimulated threshold gives $\Gamma = 25 \pm 8$ meV.[17] Thus, an increase in n by a factor of 7 increases Γ by a factor of 3.

The spin-flip scattering cross section per donor electron was determined by measuring the Raman scattered light relative to the 992-cm^{-1} mode of benzene. The scattering efficiency for benzene has been measured by Kato and Takuma[18] at $\lambda = 6328$ Å as $N(d\sigma/d\Omega) = 0.54 \times 10^{-7}$ (cm sr)$^{-1}$. A simple $(\hbar\omega_L)^4$ correction is made for the present laser wavelengths. The spin-flip scattering was found to be much stronger than the scattering from benzene. Corrections were made for sample absorption, reflectivity losses, and solid angle of collection for the backscattering geometry. Assuming the number of donors N_D equal to n, the low n sample $N_D = 3 \times 10^{16}$ cm^{-3} yields a cross section of $(d\sigma/d\Omega)_{xy} = 1.2 \times 10^{-21}$ cm^2/sr for crossed polarization (xy) at $\hbar\omega_L = 1890$ meV. The uncertainty in the cross section is estimated to be at least a factor of 2 because of the corrections and extrapolations. The oscillator strength from this cross section is $f \sim 5$. The largest cross section measured was 6×10^{-20} cm^2/sr at $\hbar\omega_L = 1945$ meV. This value is less certain because of the large absorption correction.

Scattering from paramagnetic Mn ions[19] was also observed. These $g = 2$ transitions occur within the $S = \frac{5}{2}$ multiplet of Mn^{2+}. In the $x = 0.1$ sample at $\hbar\omega_L = 1900$ meV, the integrated scattering from the Mn ions was found to be about $4\times$ that for the donor spin flip, implying $(d\sigma/d\Omega)_{xy} = 1 \times 10^{-25}$ cm^2/sr Mn-ion. Changes in the applied field and lattice temperature had little effect $(<2\times)$ on this cross section. The scattering varies with $\hbar\omega_L$ but was less dramatic compared to the donor scattering.

V. DISCUSSION

The Zeeman splitting observed in the spin-flip experiments is primarily caused by the local Mn^{2+} magnetization $\vec{M}(\vec{r})$ within the donor orbit. There are two distinct contributions to that magnetization. An external magnetic field induces a finite time average moment $\vec{M}_0$ in the Mn^{2+} spin system. In addition, even in zero field there are fluctuations

$\delta \vec{M}(\vec{r})$ of the local magnetization about its equilibrium value. $\delta \vec{M}(\vec{r})$ averages to zero over periods long compared to the spin-lattice relaxation time of the ions. However, at a given instant there is usually a finite value of $\delta \vec{M}(\vec{r})$ due to the random statistical nature of the finite spin cloud that interacts with the electron spin. Equation (29) implies that the spin-flip frequency is determined by the instantaneous magnetization $\vec{M}_0 + \delta \vec{M}$ experienced by the electron. The Mn^{2+} spin system is in effect "frozen" during the spin-flip process. This approximation, which results from our classical treatment of the Mn^{2+} spins, gives excellent results for the spin-flip spectrum. However, it cannot be used to describe Mn^{2+} spin relaxation.

The zero-field spin-flip frequency and spectrum are given by Eq. (34). At high temperatures $(\beta \omega \ll 1)$ the spectrum is determined by fluctuations; the frequency is then temperature independent. At lower temperatures $(\beta \omega \gg 1)$ the system is in the BMP regime, where the electron and Mn^{2+} spins are correlated through their mutual exchange interaction. DS have shown[6] that there is a continuous transition from the fluctuation-dominated high-temperature regime to mean-field behavior at low temperatures. The observed increase in ΔE below $T = 5$ K in the $x = 0.1$ sample is a result of the BMP interaction. However, in (Cd,Mn)Se these effects are not large. Even at $T = 1.5$ K the BMP energy is less than 10% of the total ΔE. Above $T = 5$ K the contribution from the BMP is negligible compared to that due to fluctuations. There, $\Delta E = \sqrt{2} W$ from Eq. (34).

The scattering selection rules at $B = 0$ have more allowed configurations than for large B. At $B = 0$ the major contribution to the effective magnetic field is due to thermal fluctuations in the magnetization M. The direction of $\vec{M}$ during the spontaneous donor spin flip is random. Thus scattering occurs as if all field directions were present. In certain configurations scattering occurs only at very small fields and decreases with increasing field. For example, with a backscattering wave vector $\vec{q} \perp \hat{c} \| \vec{B}$, scattering is allowed for weak fields in (xx), where $\vec{x} \perp \hat{c}$, due to fluctuations in $\vec{M}$. As the field is increased from zero, $\vec{M}$ lines up along $\vec{B}$ and the scattering be-

comes forbidden. A similar effect using circular polarization has been observed by Planel.[1]

Values for $(\alpha N_0)\bar{x}$ and T_{AF}, measured on samples from the same $x = 0.1$ boule, depend only slightly on the measuring technique. Fitting $(\partial \Delta E / \partial B)^{-1}$, or equivalently $\tilde{g}$, gives $(\alpha N_0)\bar{x} = 11.2 \pm 1.2$ meV and $T_{AF} = 3.0 \pm 0.6$ K, while low-field fits of ΔE vs B give $(\alpha N_0)\bar{x} = 11.1 \pm 1.0$ meV and $T_{AF} = 2.2 \pm 0.2$ K. Magnetization experiments of Shapira, Heiman, and Foner[10] yield $(\alpha N_0)\bar{x} = 10.1 \pm 1.0$ meV and $T_{AF} = 2.1 \pm 0.4$ K from the low-field susceptibility. The differences in $(\alpha N_0)\bar{x}$ are within experimental uncertainties.

The scattering cross section for $x = 0.10$ is resonantly enhanced as $\hbar \omega_L$ approaches $E_I = 1942 \pm 5$ meV. The largest photoluminescence peak, in the same sample, is also at this energy, at 1944 ± 5 meV. We associate this with the I_2 peak since it is usually the dominant feature in large n materials. On the other hand, the extrapolated I_2 energy is at 1979 meV, using[7] $dE_g / dx = 1.50$ eV and the I_2 energy in pure CdSe of 1821 meV.[20] These values differ by 37 ± 15 meV. If the assumption that the I_2 energy is at E_I is correct, then the difference may be associated with a BMP effect on the bound exciton. The larger effective mass of the hole produces a higher degree of localization and, hence, polaron effect. For example, the photoluminescence peak of the acceptor-bound exciton (I_1) in (Cd,Mn)Te shows a large shift with x and T.[11] There, the peak shift for $x = 0.1$ is estimated at 20 meV for $T = 2$ K.

ACKNOWLEDGMENTS

APPENDIX

To calculate the spin-spin correlation function [Eq. (2)], it is necessary to evaluate the time-dependent spin operator

$$[\vec{s}(t) \cdot \vec{\alpha}] = e^{i \mathcal{H} t}[\vec{s}(0) \cdot \vec{\alpha}] e^{-i \mathcal{H} t} . \tag{A1}$$

This task is straightforward when $\vec{\Gamma}$ is treated classically. Equation (9) then implies that the operator $[\vec{s}(t) \cdot \vec{\alpha}]$

appearing in Eq. (10) has the form

$$[\vec{s}(t)\cdot\vec{\alpha}]\simeq e^{-i(\vec{s}\cdot\vec{\gamma})t}(\vec{s}\cdot\vec{\alpha})e^{i(\vec{s}\cdot\vec{\alpha})t}\equiv e^{-i(\vec{s}\cdot\vec{\gamma})t}\left[\frac{(\vec{\gamma}\cdot\vec{\alpha})(\vec{s}\cdot\vec{\gamma})}{\gamma^2}-\frac{\vec{s}\cdot\vec{\gamma}\times(\vec{\gamma}\times\vec{\alpha})}{\gamma^2}\right]e^{i(\vec{s}\cdot\vec{\gamma})t}$$

$$=\frac{(\vec{\gamma}\cdot\vec{\alpha})(\vec{s}\cdot\vec{\gamma})}{\gamma^2}-e^{-i(\vec{s}\cdot\vec{\gamma})t}(s_\alpha^+ +s_\alpha^-)e^{i(\vec{s}\cdot\vec{\gamma})t}\ ,\qquad\text{(A2)}$$

where

$$s_\alpha^\pm\equiv\frac{1}{2}\left[\frac{\vec{s}\cdot\vec{\gamma}\times(\vec{\gamma}\times\vec{\alpha})}{\gamma^2}\pm\frac{i\vec{s}\cdot(\vec{\gamma}\times\vec{\alpha})}{\gamma}\right]\qquad\text{(A3)}$$

are stepping-up and stepping-down operators for the electron spin relative to the axis of quantization $\vec{\gamma}/|\vec{\gamma}|$. That is,

$$s_\alpha^\pm(\vec{s}\cdot\vec{\gamma})=[(\vec{s}\cdot\vec{\gamma})\pm\gamma]s_\alpha^\pm\ .\qquad\text{(A4)}$$

This relation implies that

$$[\vec{s}(t)\cdot\vec{\alpha}]=\frac{(\vec{\gamma}\cdot\vec{\alpha})(\vec{s}\cdot\vec{\gamma})}{\gamma^2}-(e^{i\gamma t}s_\alpha^+ +e^{-i\gamma t}s_\alpha^-)\ .$$

$$\text{(A5)}$$

Equation (A5) can also be derived by expanding the exponentials via the standard identity

$$e^{\pm i(\vec{s}\cdot\vec{\gamma})t}=\cos\left[\frac{\gamma t}{2}\right]\pm\frac{2i(\vec{s}\cdot\vec{\gamma})}{\gamma}\sin\left[\frac{\gamma t}{2}\right]\ ,\qquad\text{(A6)}$$

and evaluating the spin products that appear in Eq. (A2).

A complete quantum-mechanical calculation of the correlation function is much more difficult. To assess the error involved in the classical approximation, we consider the zero-field limit, where quantum-mechanical effects should be most pronounced. The formula for $S(t)$ then takes the form

$$S(t)=Z^{-1}\text{Tr}\{e^{i(\vec{s}\cdot\vec{\Gamma})t}[\vec{s}(t)\cdot\vec{\alpha}][\vec{s}(0)\cdot\vec{\alpha}^*]\}\ ,\qquad\text{(A7)}$$

where here the operator $\vec{\Gamma}$ is defined by Eq. (6), without the B_0 term. Evaluation of Eq. (A7) is complicated by the fact that Eq. (A6) fails when the c number $\vec{\gamma}$ is replaced by the operator $\vec{\Gamma}$. Equation (A7) is derived by power-series expansion of the exponential and repeated applications of the identity

$$(\vec{s}\cdot\vec{\gamma})^2=\frac{\gamma^2}{4}\ .\qquad\text{(A8)}$$

When $\vec{\gamma}\rightarrow\vec{\Gamma}$, Eq. (A8) is replaced by the more complicated form

$$(\vec{s}\cdot\vec{\Gamma})^2=\frac{\Gamma^2}{4}+\frac{i}{2}\vec{s}\cdot(\vec{\Gamma}\times\vec{\Gamma})$$

$$=\left[\frac{\Gamma^2}{4}-\frac{\vec{s}}{2}\cdot\sum_j(K_j^2\vec{S}_j)\right]\ ,\qquad\text{(A9)}$$

and the simple identity no longer holds.

The problem is enormously simplified via the drastic approximation

$$K_j=K=\text{const}\ ,\qquad\text{(A10)}$$

$$\vec{\Gamma}=K\sum_j^N(\vec{S}_j)\ .$$

$\vec{\Gamma}$ then commutes with Γ^2, and Eq. (A9) can be rewritten in the form

$$\left[(\vec{s}\cdot\vec{\Gamma})+\frac{K}{4}\right]^2=\left[\frac{\Gamma^2}{4}+\frac{K^2}{16}\right]\ .\qquad\text{(A11)}$$

It then follows that

$$e^{i(\vec{s}\cdot\vec{\Gamma})t}=\exp\left[\frac{\pm iKt}{4}\right]\exp\left[\pm i\left[(\vec{s}\cdot\vec{\Gamma})+\frac{K}{4}\right]t\right]\equiv e^{\pm iKt/4}\left[\cos\left[\frac{\beta\Omega}{2}\right]\pm\frac{2i[(\vec{s}\cdot\vec{\Gamma})+K/4]}{\Omega}\sin\left[\frac{\beta\Omega}{2}\right]\right]\ ,$$

$$\text{(A12)}$$

with

$$\Omega^2\equiv\left[\Gamma^2+\frac{K^2}{4}\right]\ .\qquad\text{(A13)}$$

Note that the power-series expansions of the two functions appearing in Eq. (A12) involve only even powers of Ω; thus it is never necessary to take the square root of Eq. (A13). It is now a straightforward (though tedious) task with the aid of Eq. (A12) and the corresponding expression for $e^{\beta(\vec{s}\cdot\vec{\Gamma})}$ to perform the trace over s in Eq.

(A7). The positive frequency portion of the resulting expression has the form

$$\frac{1}{4}\left[(\vec{a}\cdot\vec{a}^{*})-\frac{1}{2\Gamma^{2}}(\vec{a}\cdot\vec{\Gamma})(\vec{a}^{*}\cdot\vec{\Gamma})+(\vec{a}^{*}\cdot\vec{\Gamma})(\vec{a}\cdot\vec{\Gamma})-\frac{i\vec{\Gamma}\cdot(\vec{a}\times\vec{a}^{*})}{\Gamma}\right]e^{i\Omega t}e^{-\beta\Omega}$$

$$+\left[\frac{K}{8\Gamma}\right]\left[(\vec{a}\cdot\vec{a}^{*})+\frac{1}{2\Gamma^{2}}[(\vec{a}\cdot\vec{\Gamma})(\vec{a}^{*}\cdot\vec{\Gamma})+(\vec{a}^{*}\cdot\vec{\Gamma})(\vec{a}\cdot\vec{\Gamma})]\right]e^{i\Omega t}\sinh\left[\frac{\beta\Omega}{2}\right]. \quad (A14)$$

The first term in this formula is equivalent to the first term of Eq. (16) with the replacement $\vec{\gamma}\rightarrow\vec{\Gamma}$. The correction is of order $(K/8\Gamma)$. As indicated by Eq. (25), the rms value of $\vec{\Gamma}$ is

$$\langle\Gamma^{2}\rangle^{1/2}\simeq W=N^{1/2}K, \quad (A15)$$

a result suggesting that the classical approximation (for this simple model of the BMP) is accurate to order $N^{-1/2}$.

[1]See the following review articles: R. R. Gałazka, in *Proceedings of the XIV International Conference on the Physics of Semiconductors, Edinburgh, 1978*, edited by B. C. H. Wilson (IOP, Bristol, 1978), p. 133; J. A. Gaj, in Proceedings of the XV International Conference on the Physics of Semiconductors, Kyoto, 1980 [J. Phys. Soc. Jpn. Suppl. A 49, 797 (1980)]; T. Dietl, in *Physics in High Magnetic Fields*, Vol. 24 of the *Springer Series in Solid State Sciences*, edited by M. Miura (Springer, Berlin, 1981), p. 344; J. K. Furdyna, in Proceedings of the 3rd Joint Intermag—Magnetism and Magnetic Materials Conference, Montreal, 1982 [J. Appl. Phys. 53, 7637 (1982)]; A. K. Ramdas, *ibid.*, p. 7649; J. Mycielski, in Proceedings of the International Conference on the Application of High Magnetic Fields in Semiconductor Physics, Grenoble, 1982 (in press); R. Planel, *ibid.*

[2]R. R. Gałazka, S. Nagata, and P. H. Keesom, Phys. Rev. B 22, 3344 (1980); S. B. Oseroff, *ibid.* 25, 6584 (1982), and references cited therein.

[3]F. F. Geyer and H. Y. Fan, IEEE J. Quantum Electron. QE-16, 1365 (1980).

[4]M. Nawrocki, R. Planel, G. Fishman, and R. Gałazka, in Proceeings of the XV International Conference on the Physics of Semiconductors, Kyoto, 1980 [J. Phys. Soc. Jpn. Suppl. A 49, 823 (1980)]; Phys. Rev. Lett. 46, 735 (1981).

[5]M. Dobrowolska, H. D. Drew, J. K. Furdyna, T. Ichiguchi, A. Witowski, and P. A. Wolff, Phys. Rev. Lett. 49, 845 (1982).

[6]T. Dietl and J. Spałek, Phys. Rev. Lett. 48, 355 (1982).

[7]J. Stankiewicz, Phys. Rev. B 27, 3631 (1983).

[8]D. Heiman, P. A. Wolff, and J. Warnock, in Proceedings of the XVI International Conference on the Physics of Semiconductors, Montpellier, France. 1982 (in press).

[9]J. A. Gaj, R. Planel, and G. Fishman, Solid State Commun. 25, 193 (1978).

[10]Y. Shapira, D. Heiman, and S. Foner, Solid State Commun. 44, 1243 (1982).

[11]A. Golnik, J. A. Gaj, M. Nawrocki, R. Planel, and C. Benoît à la Guillaume, in Proceedings of the XV International Conference on the Physics of Semiconductors, Kyoto, 1980 [J. Phys. Soc. Jpn. Suppl. A 49, 819 (1980)].

[12]P. A. Wolff, J. C. Ramos, and S. Yuen, *Theory of Light Scattering in Condensed Matter*, edited by Bernard Bendow, Joseph L. Birman, and Vladimir M. Agranorich (Plenum, New York, 1977).

[13]R. Romestain, S. Geschwind, and G. E. Devlin, Phys. Rev. Lett. 35, 803 (1975).

[14]L. D. Landau and E. M. Lifshitz, *Statistical Physics* (Pergamon, New York, 1977), Chap. 12.

[15]D. G. Thomas and J. J. Hopfield, Phys. Rev. 175, 1021 (1968).

[16]J. F. Scott, T. C. Damen, and P. A. Fleury, Phys. Rev. B 6, 3856 (1972).

[17]D. Heiman, Appl. Phys. Lett. 41, 585 (1982).

[18]Y. Kato and H. Takuma, J. Chem. Phys. 54, 5398 (1971).

[19]A. Petrou, D. L. Peterson, S. Venugopalan, R. R. Gałazka, A. K. Ramdas, and S. Rodriguez, Phys. Rev. Lett. 48, 1036 (1982).

[20]C. H. Henry, K. Nassau, and J. W. Shiever, Phys. Rev. B 5, 458 (1972).